World Applied Sciences Journal 29 (12): 1649-1660, 2014
ISSN 1818-4952

DOI: 10.5829/idosi.wasj.2014.29.12.14470

Modeling and Simulation for Variable Speed Direct Drive Wind Energy Conversion System with Electrically Excited Synchronous Generator

[1]W.I.Mohamed, [2]A.M. Ibrahim, [1]M.N.Eskander and [2]H.T. Dorra

[1]Electronics Research Institute, Dokki, Giza, Egypt
[2]Faculty of Engineering, Cairo University, Giza, Egypt

Abstract: Nowadays Direct drive variable speed Wind Energy Conversion System (WECS) are increasing rapidly due to the proper performance and the better reliability than the geared drives. In direct drive WECS, the generator is either Permanent Magnet Synchronous Generator (PMSG) or Electrically Excited Synchronous Generator (EESG). Both generators have advantages and disadvantages. In this paper, the comparison between PMSG and EESG for WECS shall be presented. Moreover, complete modeling and simulation for WECS based on EESG system shall be presented. The mathematical equations for each subsystem and the control strategies for each subsystem are fully described.

Key words: Control . converter . EESG . MATLAB . PMSG . simulation . variable speed

INTRODUCTION

Wind energy has undergone a revolution during the last century. A renewed interest in wind energy arose during the oil crisis in the mid 1970s. This attention has continued to grow as the demands on reducing polluting emissions have increased as well as the expected oil crisis in the future. The wind power industry has experienced an average growth rate of 27% per year between 2000 and 2011. The wind power capacity at the end of 2011 reached 238 GW by the end of 2011 as shown in Fig. 1 [1]. Direct drive synchronous generator either EESG or PMSG has the capability of direct connection (direct-drive) to wind turbines with no gearbox. This advantage is favorable with respect to lifetime and maintenance specially in high wind speeds conditions. In the recent years the use of direct drive machines with full scale power converters is increasing than before because of the numerous advantages from grid connection point of view and the fulfilling for all the international grid code requirements. In addition to that the cost of power electronics is also decreasing. Furthermore, the variable speed direct-drive machines with a full-scale power converter becoming the first choice for offshore wind farms [2]. In Polinder *et al*. [3] a comparisons among the different WECS in terms of energy production and the cost per kWH based on real market prices has been provided. Furthermore, In Polinder *et al*. [4], a comparison among the different WECS based on Doubly Fed Induction Generator (DFIG), EESG and PMSG in terms of reliability, operation and maintenance have been provided. The comparison between PMSG and EESG could be summarized as follows:

- PMSG has higher efficiency and energy yield.
- PMSG has no field losses like EESG.
- PMSG has no slip rings like EESG and accordingly PMSG is completely closed generator with higher protection degree while EESG is open generator concept with lower protection degree.
- PMSG is lighter and therefore higher power to weight ratio.
- Permanent magnet production is nearly denominated by china [5] and this is expected to continue in the future as shown in Fig. 2. On the other hand, EESG is consisting of copper bars which are available anywhere.
- Expected jump in the magnet price [5] as shown in Fig. 3 due to the sole supplier and the shortage due to gap between the supply and demand.
- EESG has no difficulties to handle in manufacturing like PMSG.
- EESG has no difficulties in maintenance on site like PMSG.
- Demagnetization of PM at high temperature is a severe problem, EESG has no demagnetization problems.

In conclusion, EESG is the better choice in regions which have climate characterized by high wind speeds

Corresponding Author: W.I. Mohamed, Electronics Research Institute, Dokki, Giza, Egypt

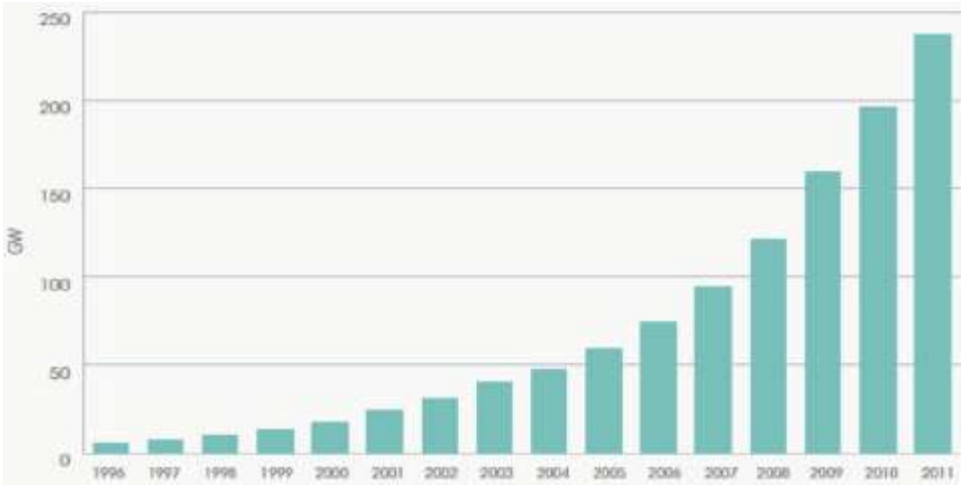

Fig. 1: Global installed wind power capacity, 1996 to 2011

Fig. 2: World magnet production by region from 2005 to 2020

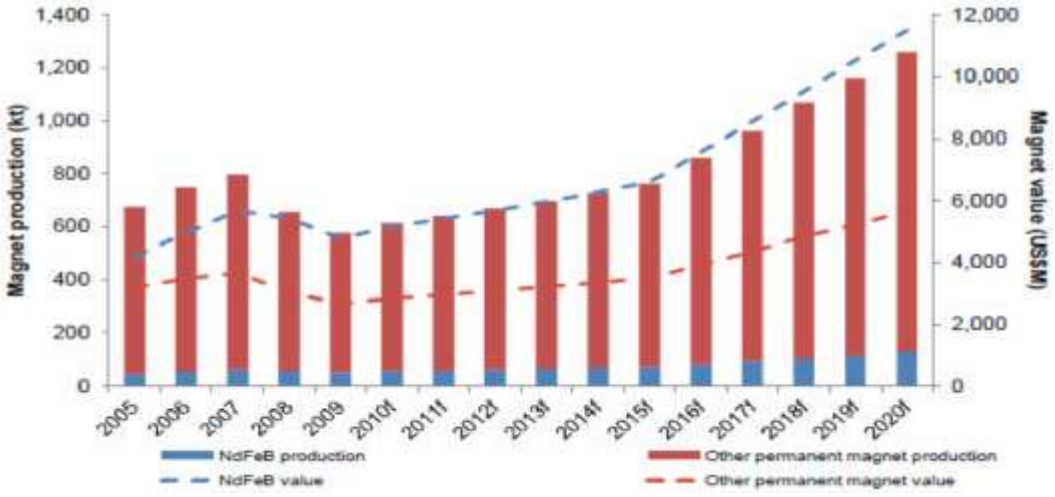

Fig. 3: Magnet price growth

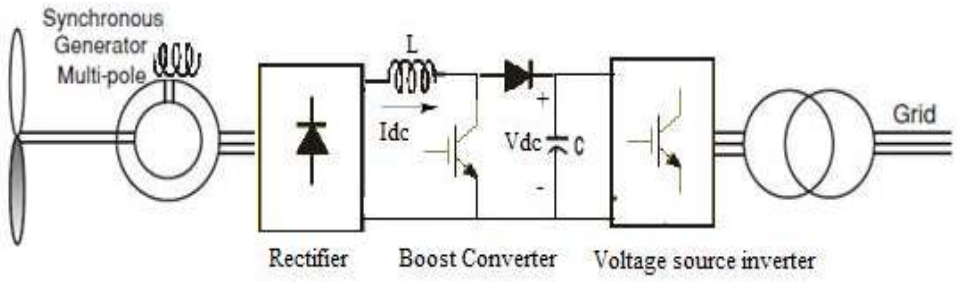

Fig. 4: WECS with EESG

with high temperature to gather the benefits from the direct drive technology in high wind speeds and to avoid the demagnetization problem for the PMSG in high temperatures. On the other hand, PMSG is the better choice in regions which have climate characterized by high wind speeds and low temperature to gather the benefits from the direct drive technology in high wind speeds and to maximize the energy production. On contrary of DFIG and PMSG, the available literature for WECS based on EESG is very rare. Furthermore, most of published works for direct drive systems proposing the back to back voltage source converter with vector control techniques in machine side and grid side. This paper present direct drive wind energy conversion system based on EESG. The AC/DC/AC converter is comprises of uncontrolled diode rectifier followed by boost converter and IGBT inverter. The control strategies for each subsystem shall be fully described.

System modeling: The system is shown in Fig. 4 direct drive grid connected wind turbine with multi-pole field excited synchronous generator equipped with generator side diode rectifier, DC boost converter and grid side converter. The control goals could be listed as follow:

- Maximum power point extraction in the below rated wind speed.
- Power limitation through pitch control.
- Field excitation control.
- Vector controlled current regulator inverter for synchronization to grid with controlled power factor.

Wind turbine: The mechanical power output of this turbine can be written as:

$$P_m = 0.5\, p\, \rho\, C_P\, R^2\, V_w^3 \quad (1)$$

where power coefficient Cp is related to tip speed ratio λ by a non linear relation as shown in Fig. 5 and

$$\lambda = \omega R / V_w \quad (2)$$

The aerodynamic torque is given by:

$$T_w \frac{0.5\,\pi\,\rho\, C_p R^3 V_w^2}{\lambda} = 0.5\,\pi\,\rho\, C_T R^3 V_w^2 \quad (3)$$

$$C_T = C_p / \lambda \quad (4)$$

As shown in Fig. 5, the performance coefficient will reach its maximum value when the pitch angle is zero and then tip speed ratio resulted from this is the nominal value.

Multi-pole synchronous generator: The generator is represented in rotationally rotor reference frame (dq frame) and all the electrical quantities are seen from the stator. The equivalent circuits of the generator in (dq frame) are shown in Fig. 6 and 7. The generator equations could be written as Ion Boldea [6]:

$$V_d = R_s i_d + \frac{d}{dt}\varphi_d - \omega\varphi_q \quad (5)$$

$$V_q = R_s i_q + \frac{d}{dt}\varphi_q + \omega\varphi_d \quad (6)$$

$$V'_{fd} = R'_{fd} i'_{fd} + \frac{d}{dt}\varphi'_{fd} \quad (7)$$

$$V'_{kd} = R'_{kd} i'_{kd} + \frac{d}{dt}\varphi'_{kd} \quad (8)$$

$$V'_{kq1} = R'_{kq} i'_{kq1} + \frac{d}{dt}\varphi'_{kq1} \quad (9)$$

$$V'_{kq2} = R'_{kq2} i'_{kq2} + \frac{d}{dt}\varphi'_{kq2} \quad (10)$$

$$\varphi_d = L_d i_d + L_{md}(i'_{fd} + i'_{kd}) \quad (11)$$

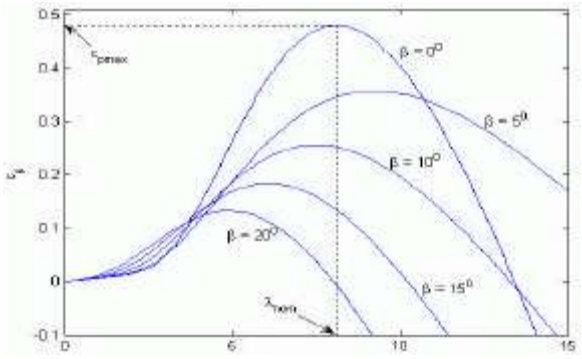

Fig. 5: Cp as a function of pitch angle and tip speed

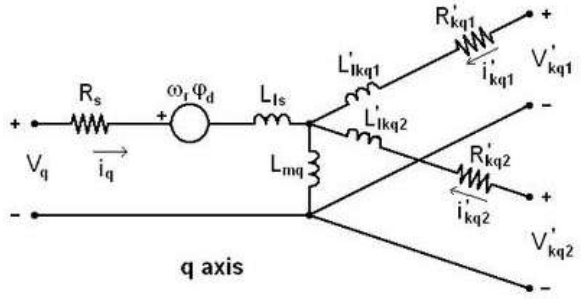

Fig. 6: The electrical model of the generator related to q axis

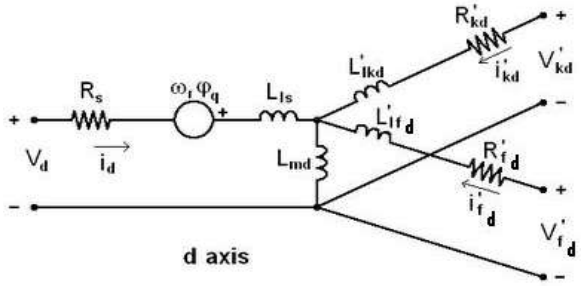

Fig. 7: The electrical model of the generator related to d axis

$$\varphi_q = L_q i_q + L_{mq} i'_{kq} \quad (12)$$

$$\varphi'_{fd} = L'_{fd} i'_{fd} + L_{md}(i_d + i'_{kd}) \quad (13)$$

$$\varphi'_{kd} = L'_{kd} i'_{kd} + L_{md}(i_d + i'_{fd}) \quad (14)$$

$$\varphi'_{kq1} = L'_{kq1} i'_{kq1} + L_{mq} i_q \quad (15)$$

$$\varphi'_{kq2} = L'_{kq2} i'_{kq2} + L_{mq} i_q \quad (16)$$

(AC/DC/AC) converter modeling and control: As shown in Fig. 4, the AC/DC/AC converter is consisting

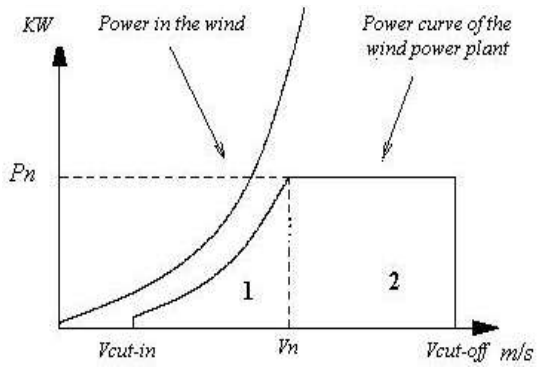

Fig. 8: Different region for wind speed (Vs) power curve

of a diode rectifier, a boost DC/DC converter and a DC/AC voltage-source inverter (VSI). The boost converter comprises an inductor, an IGBT switch, a diode and the output capacitor. The boost converter shall be responsible for controlling the generator output power in the below rated speed region (maximum power tracking). VSI converts the DC power coming from the DC bus to AC with specific voltage and frequency to meet the grid requirements.

Control for maximum power tracking: Different regions for wind speed-power curve are shown in Fig. 8. The control strategy depends on each region nature.

Region 1: [Vcut in... Vn] Maximization of extracted energy: the wind turbine should extract wind energy at the highest efficiency.

Region 2: [Vn... Vcut off] Limitation of extracted energy: the controls aim to keep the generator output power at the nominal power Pn by pitching the blades.

In each of the following regions the reference turbine speed in rad/sec and the reference torque shall be calculated using equations 1, 2, 3, 4 and Fig. 5.

Speed control in region 1:

In Fig. 5, the condition for maximum power tracking is at the maximum point of the curve (λ_m, C_{Pmax}). At this point:

$$\omega_{ref} = \lambda_m V_w / R = K_1 V_w \quad (17)$$

$$T_{ref} = 0.5\,\pi\,\rho\; C_{P\,max}\; R^3\,\omega_{ref}^2 R^2/\lambda_m^3 = K_2\omega_{ref}^2 \quad (18)$$

where:

$$K_1 = \lambda_m / R \quad (19)$$

$$K_2 = 0.5\,\pi\,\rho\; C_{P\,max}\; R^5/\lambda_m^3 \quad (20)$$

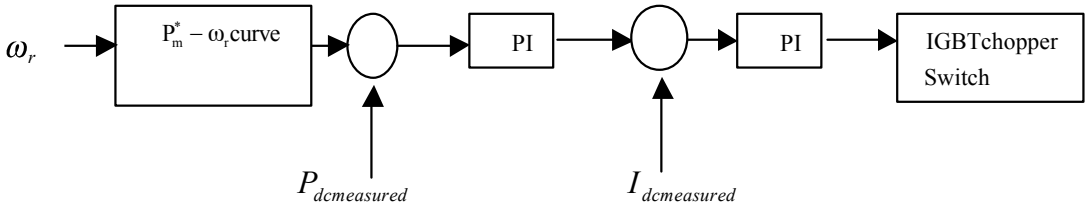

Fig. 9: Speed controller block diagram

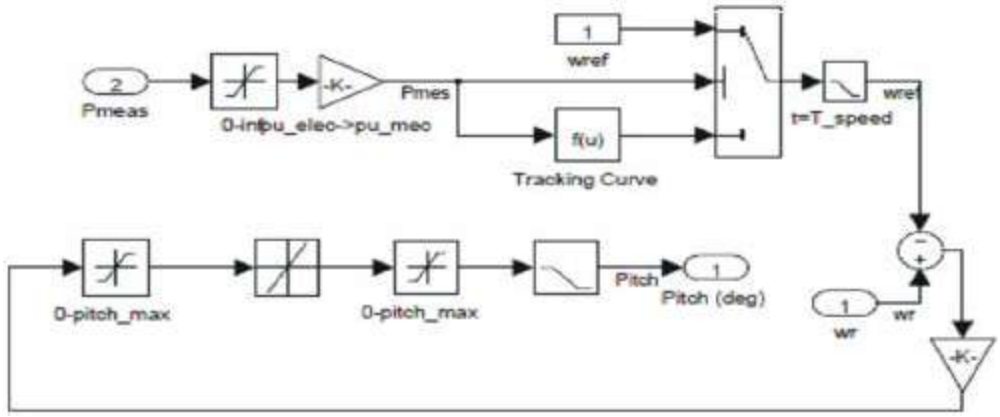

Fig. 10: Pitch controller block diagram

Different formulas have been developed for (λ, C_P, β) [7, 8]. The following formula will be used:

$$C_P = C_1 (C_2/\lambda_i - C_3\beta - C_4)e^{-C_5/\lambda_i} + C_6 \lambda \quad (21)$$

Where

$$\frac{1}{\lambda_i} = \frac{1}{\lambda + 0.08\beta} - \frac{0.035}{\beta^3 + 1} \quad (22)$$

The coefficients C_1 to C_6 are 0.517, 116, 0.4,5, 21, 0.0068, respectively.

However, by substituting the value of C_p ($C_{p\,max}$) = 0.48 in (1), the result will be the optimal mechanical power for each wind speed (rotor speed).

The C_p-λ characteristics, for different values of the pitch angle β are shown in Fig. 5. The maximum value of C_p is achieved for ß = 0 degree and for λ = 8.1. This particular value of λ is defined as the nominal value (λ_{nom}). Referring to Fig. 4, the following equation could be deducted.

$$P_m^* = P_{dc}^* \quad (23)$$

Neglecting the losses in the diode rectifier. Moreover, the measured DC power shall be tracked to the reference generator power (as described above) and the error will be the input to the DC current controller which in turn generates the gating signals for the DC chopper switch. The controller block diagram as shown in Fig. 9.

Pitch control: For region 2 in Fig. 8 no optimization for wind power is done and the power is limited to the nominal power of the generator by means of pitch regulation. The controller receives the measured output power of the generator and compares this power with nominal power of the generator to decide the region of control and which route shall be followed (If $P_{measured} \geq P_{nominal}$ go to region 2 algorithm otherwise, go to region 1 algorithm.) As shown in Fig. 10. The reference rotor speed will be specified accordingly and compared to the measured rotor speed; the positive error drives the pitch mechanism to higher angles. A rate limiter, set at 10 deg/s is used.

Flux estimation and field control: The three phase stator currents, voltages and the rotor angle shall be measured and the stator currents and the stator voltages are transformed into the stationary two axes ($\alpha\beta$) Coordinate system and then into the rotating (dq) coordinate system. From equations (7) and (8), the magnitude of flux could be estimated as follow:

$$\varphi_d = (V_q - R_s i_q) / \omega_r \quad (24)$$

$$\varphi_q = (V_d - R_s i_d) / -\omega_r \quad (25)$$

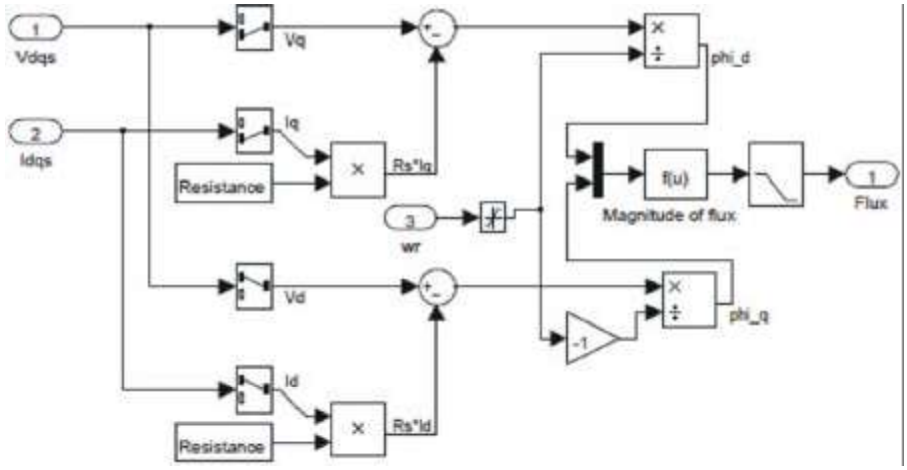

Fig. 11: Flux estimation block diagram

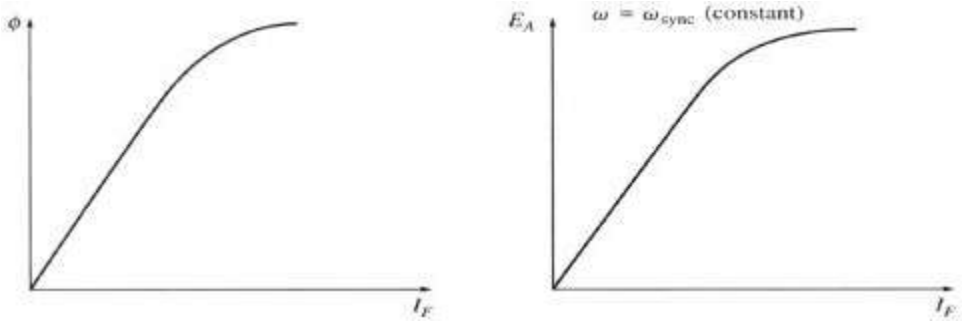

Fig. 12: Magnetization of a synchronous machine

From (24) & (25), the magnitude of flux can be calculated:

$$|\varphi| = \sqrt{\varphi_d^2 + \varphi_q^2} \tag{26}$$

The block diagram for the flux estimation is shown in Fig. 11.

For the synchronous machine, the magnitude of internal generated voltage induced in a stator is related to the machine flux and rotor speed [9].

$$E_A = \sqrt{2}\pi N_c \varphi f = K\varphi\omega \tag{27}$$

where, K is a constant representing the construction of the machine, ϕ is flux in it and ω is its rotation speed. Since flux in the machine depends on the field current through it, the internal generated voltage is a function of the field current (voltage) as shown in Fig. 12.

From equation (27) and the linear relation between the flux and the field current as well as the linear relation between the induced voltage and the field current, the following relations could be deduced:

$$E_A = KV_f\omega \tag{28}$$

$$\varphi = K_1 V_f \tag{29}$$

From equations (28) and (29), the flux reference has been adjusted according to the measured rotation speed since the flux is inversely related to the rotation speed. The estimated flux obtained from equation (26) is then tracked to the reference flux while the error is entering to PI controller resulting to the field excitation voltage. The field excitation controller block diagram is shown in Fig. 13.

Grid side converter (DC/AC) control: The control system for the vector controlled grid-connected converter consists of two control loops. The inner control loop controls the active and the reactive grid current components while the outer control loop determines the active current reference by controlling the direct voltage. The reactive current reference for a grid connected converter is defined for controlling the power factor [10, 11]. The vector control of a grid

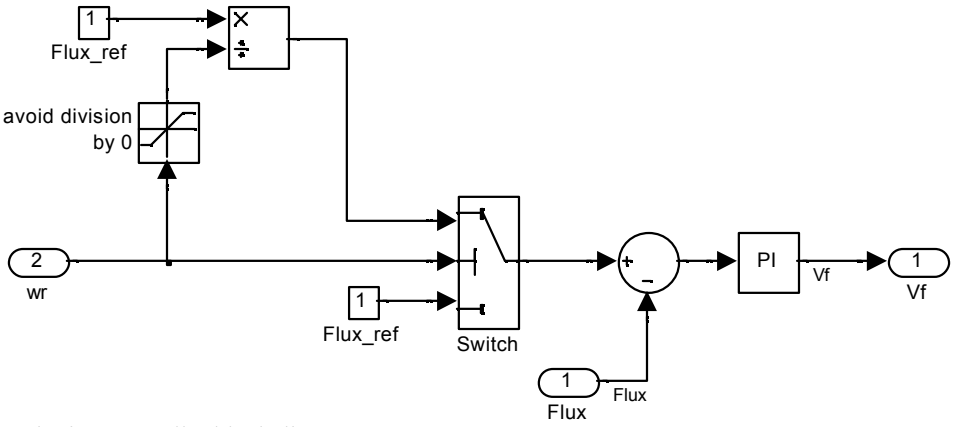

Fig. 13: Field excitation controller block diagram

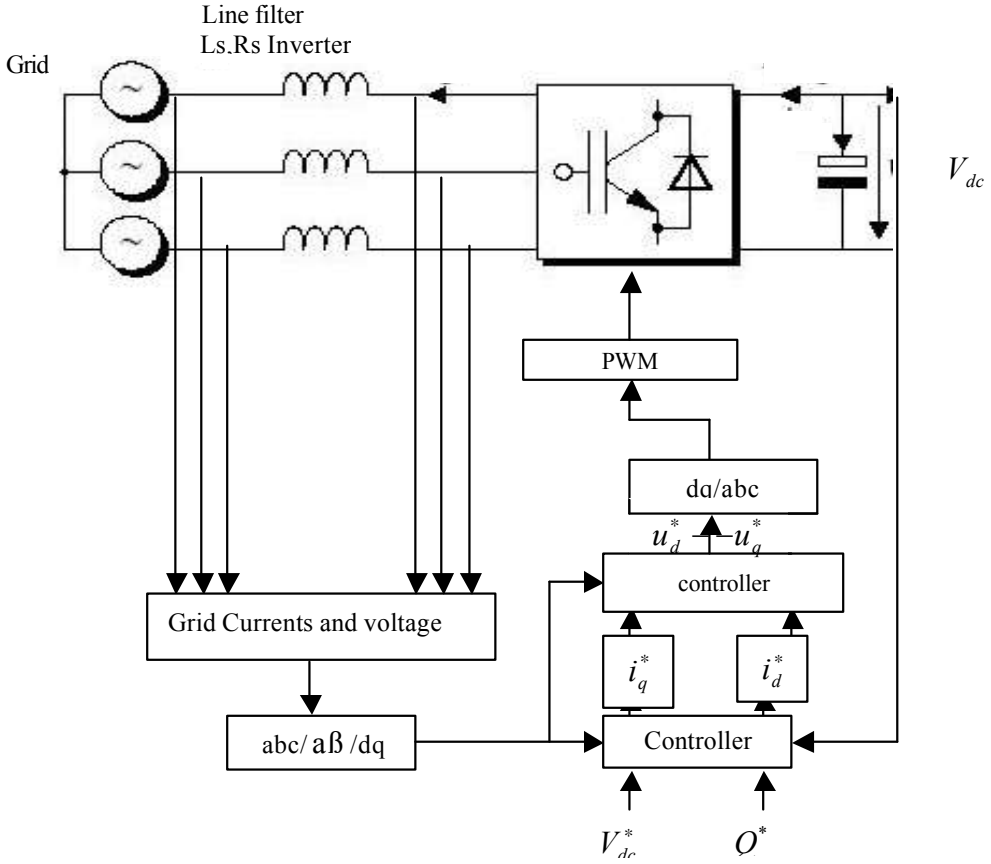

Fig. 14: Block diagram for vector control of grid connected inverter

connected converter is shown in Fig. 14. The grid currents and the grid voltages are transformed into the stationary two axis (aß) Coordinate system and then into the rotating (dq) coordinate system. The grid voltage vector occurs in the q-direction. The coordination on d-q frame is shown in Fig. 15 where:

$$\cos\theta_g = \frac{e_ß}{e_q}, \sin\theta_g = -\frac{e_a}{e_q} \quad (30)$$

The direct axis current corresponds to reactive power while the quadrature axis current corresponds to active power. The reactive and active power can therefore be controlled independently since the current components are orthogonal.

DC-voltage controller (Outer control loop): Based on Fig. 14, the instantaneous apparent power flowing into the grid can be written as:

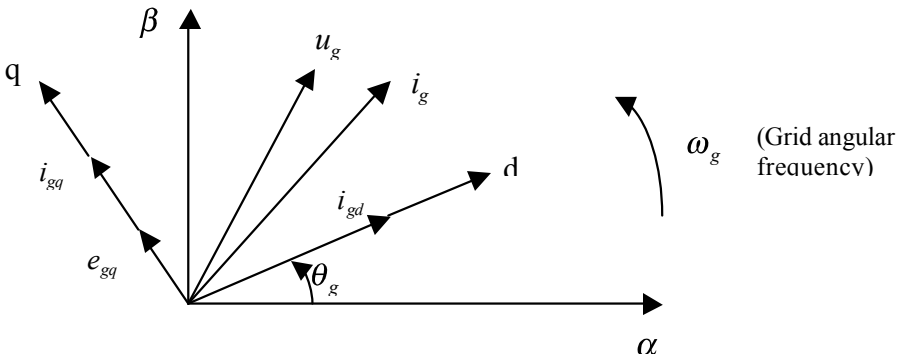

Fig. 15: The coordination on d-q frame

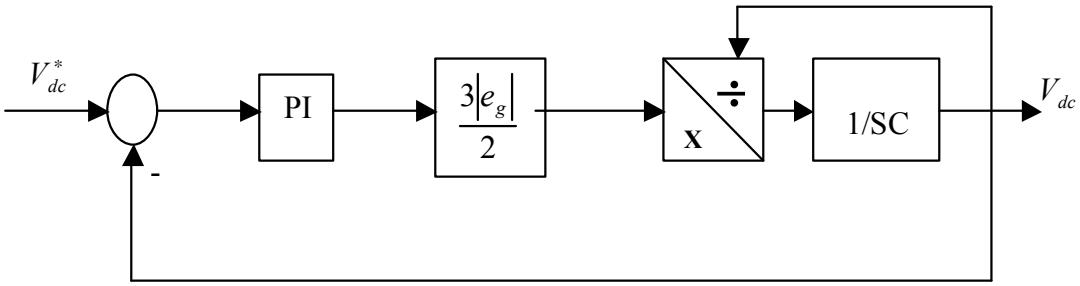

Fig. 16: Block diagram for the DC voltage controller (outer control loop)

$$S_g = P_g + jQ_g = \frac{3}{2} e_g^{dq} i_g^{dq*} = \frac{3}{2}(e_{gq} i_{gq} + j e_{gq} i_{gd}) \quad (31)$$

The active power is the real part of (31), thus

$$P_g = \frac{3}{2}\left|e_{gq}\right| i_{gq} \quad (32)$$

The DC voltage link power is given by:

$$P_{dc} = V_{dc} i_{dc} = V_{dc} C \frac{dV_{dc}}{dt} \quad (33)$$

Assuming that the converter losses can be neglected, the power balance in the DC voltage link can be written as:

$$V_{dc} C \frac{dV_{dc}}{dt} = \frac{3}{2}\left|e_{gq}\right| i_{gq} \quad (34)$$

So, a transfer function between the direct voltage and active grid current can be obtained as:

$$\frac{V_{dc}}{i_{gq}} = \frac{3\left|e_q\right|}{2pCV_{dc}} \quad (35)$$

The transfer function is non-linear; the linear transfer function could be obtained by substituting V_{dc} by its reference value since the objective is to maintain a constant DC voltage. So, the transfer function can be written as:

$$\frac{V_{dc}}{i_{gq}} \approx \frac{3\left|e_q\right|}{2pCV_{dc}^*} \quad (36)$$

The block diagram for the outer control loop is shown in Fig. 16.

Open-loop Reactive Power Control: The reactive power exchange with the grid is controlled by the reactive current component. The simplest method to control the reactive power is via an open-loop. Taking the imaginary part of equation (31) gives the reactive reference current as:

$$i_{gd}^* = \frac{2}{3e_{gq}} Q_g^* \quad (37)$$

The reactive current reference could set to zero for unity power factor.

Current control loop (Inner control loop): Referring to Fig. 14, the equations for the grid and inverter voltages could be written as follow:

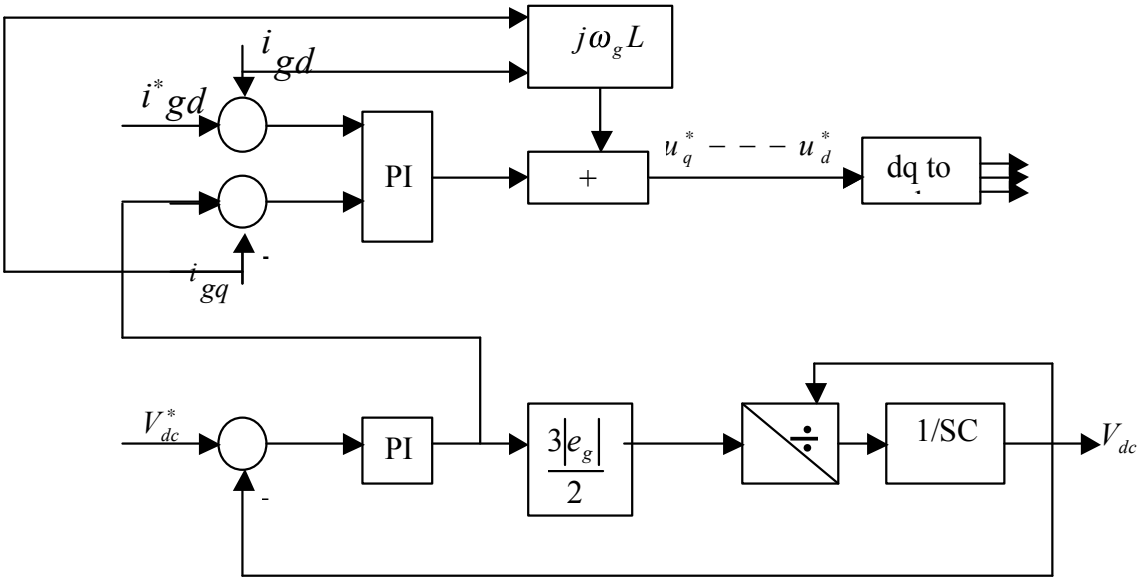

Fig. 17: Control loops for vector controlled grid connected inverter

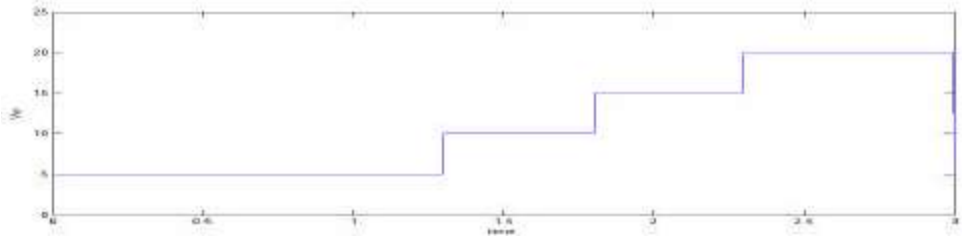

Fig. 18: Wind speed

$$u_g(t) - e_g(t) = i(t)R_s + L_s\frac{di(t)}{dt} \tag{38}$$

in d-q frame:

$$u_d - e_{gd} = i_{gd}R_s + L_s\frac{di_{gd}}{dt} + j\omega_g L_s i_{gq} \tag{39}$$

$$u_q - e_{gq} = i_{gq}R_s + L_s\frac{di_{gq}}{dt} + j\omega_g L_s i_{gd} \tag{40}$$

By substituting, $i_{gq} = i_{gq}^*$, $i_{gd} = i_{gd}^*$ and $e_{gd} = 0$, The control block diagram is shown in Fig. 17.

SIMULATION RESULTS

MATLAB/Simulink with Simpower system blocksets-Version 2011R software package is used for system simulation to study the response of the proposed grid connected wind turbine synchronous generator system at random wind speed input. The response of different control techniques are studied to show the effect of the controllers and the proper dynamic response. All the turbine parameters, generator parameters and converter parameters are given in Appendix 1). In Fig. 18 the input wind speed has been started with 5 m/s then 10 m/s, 15m/s and 20m/s. This will clarify the response of different controllers to track the wind speed variation. Figure 19 showing the grid voltages and Fig. 20, showing the current amplitudes variation based on the wind speed variations (Fig. 21 and 22) showing the stator voltage and stator currents. The stator current amplitude variation is due to the wind speed variations. Figure 23 showing the active power and in Fig. 24, the reactive power has been tracked successfully to the reference values whatever the wind speed value. In Fig. 25, the DC link voltage has been tracked successfully to the reference value for all wind speed values. In Fig. 27, the pitch degree is nearly zero corresponding to the 5m/s wind speed because in low wind speed region the rotor speed is tracked to wind speed according to Cp-λ curve (maximum power tracking) while for higher wind

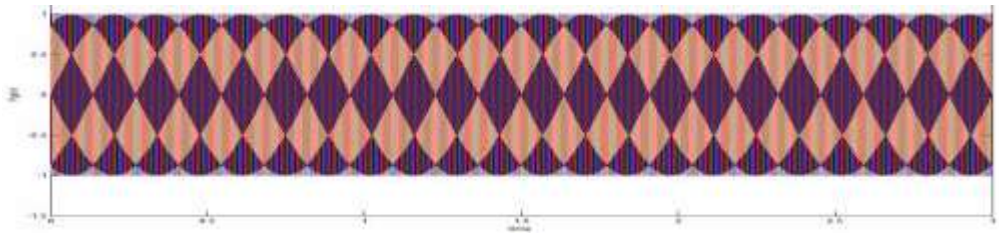

Fig. 19: Grid voltages

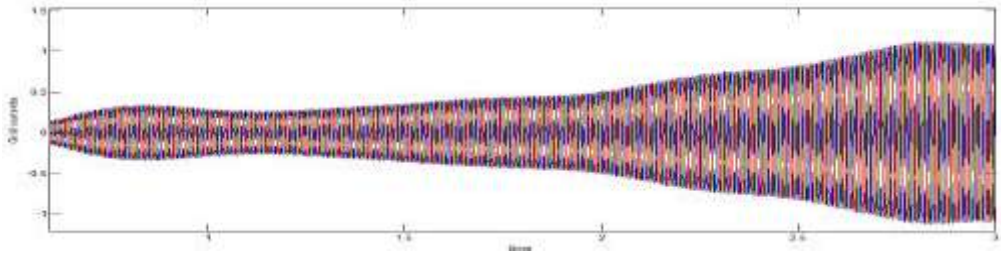

Fig. 20: Grid currents

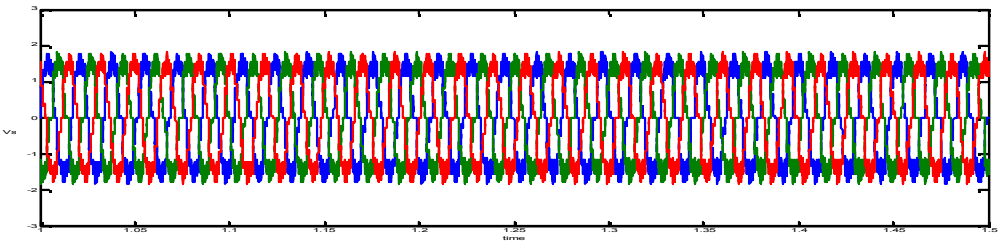

Fig. 21: Stator voltage

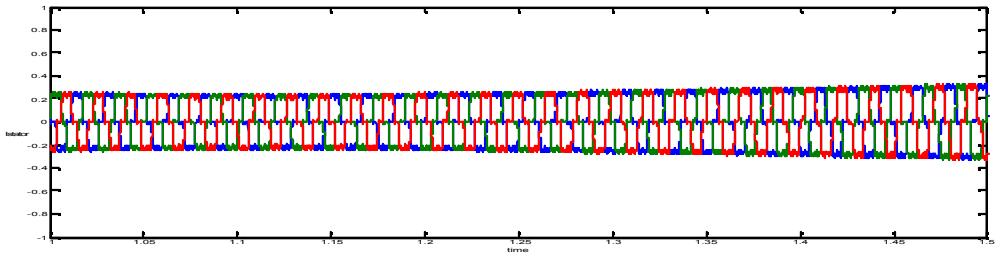

Fig. 22: Stator currents

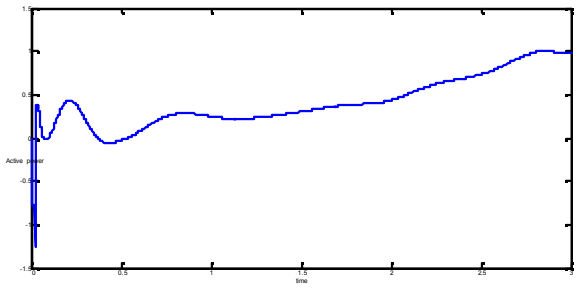

Fig. 23: Active power

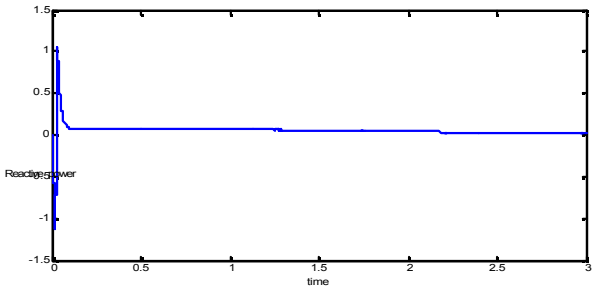

Fig. 24: Reactive power

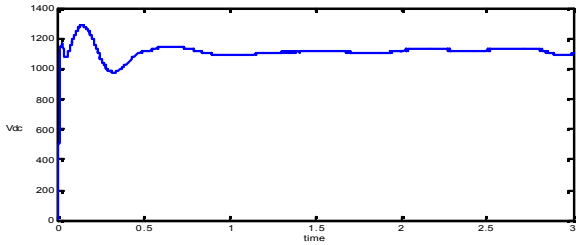

Fig. 25: DC voltage

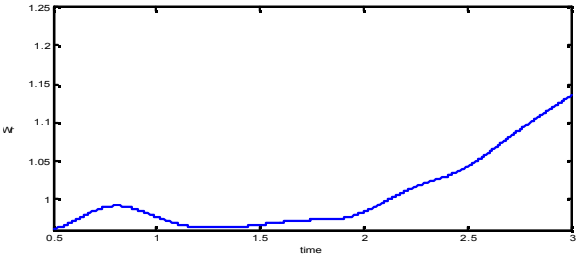

Fig. 26: Rotor speed

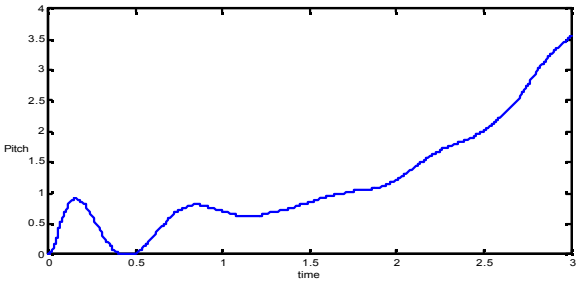

Fig. 27: Pitch angle

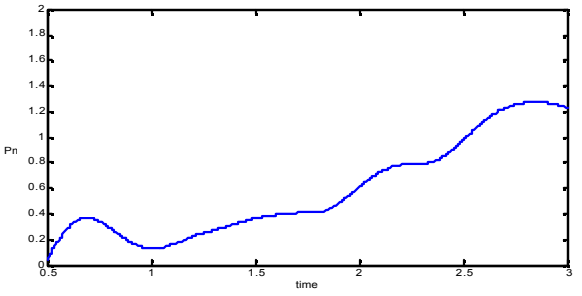

Fig. 28: Mechanical power

speeds the pitch angle starting to increase to regulate the power output. Figure 26, 28 and 29 showing the rotor speed behavior and consequently the field voltage and mechanical power output which are follows the rotor speed reflecting the proper operation of the field controller. Figure 30 showing the dc link current which is following the rotor speed which reflecting the proper operation of speed controller.

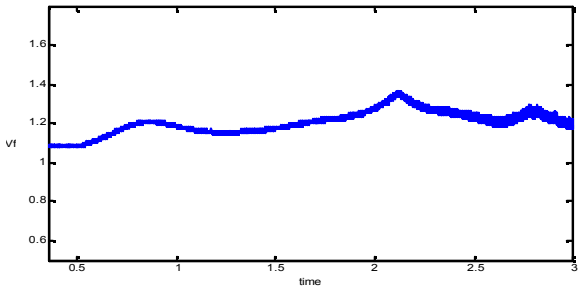

Fig. 29: Field voltage

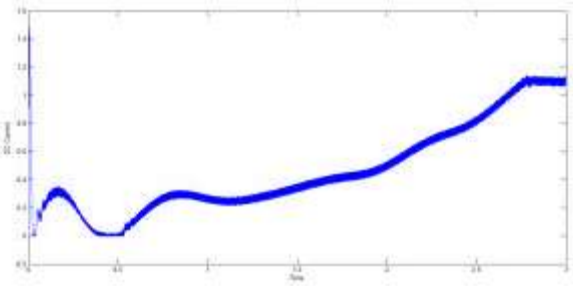

Fig. 30: DC current

Appendix 1

Turbine data:

Horizontal Axis	
Rotor Diameter	= 77 m
Hub Height	= 71 m
Rated Electrical Power	= 1.65 MW at 15m/s
Tip speed	= 73 m/s
Cut-in wind speed	= 3.5 m/s
Cut out wind speed	= 25 m/s
Swept area	= 4654.20 m^2
Design Tip Speed	= 6.1

Generator data

xd (pu)	= 0,807
xq (pu)	= 0,449
X'd (pu)	= 0,296
X''d (pu)	= 0,201
x''q (pu)	= 0,233
Xbase	= 0.2278 O
Internal impedance: Rphase	= 17.54 mO,
Ld = 3.29 mH, Lq	= 1.79 mH

Converter

Boost converter Inductance	= 0.0012 H
Boost converter Resistance	= 5e-3
DC link capacitor	= 90000e-6
Nominal DC link voltage	= 1100V
Nominal Voltage	= 690 V
Excitation nominal voltage	= 700V
Excitation nominal current	= 120A
Inertia constant	= 4.32 S
Nominal rotor speed	= 18 RPM
Nominal power	= 1.65 MW
Number of poles	= 60

Nomenclature

V_w	Wind speed (m/s)
T_w	Aerodynamic torque of wind turbine
P_m	Mechanical output power
C_P	Power coefficient of rotor blades
C_T	Torque coefficient of rotor blades
λ	Tip speed ratio
ß	Pitch angle
V_q, i_q	Quadrature axis voltage and current
V_d, i_d	Direct axis voltage and current
f_q, f_d	Stator quadrature and direct axis fluxes
Rs	Stator resistance
Lmd	Direct-axis magnetizing inductance
Lmq	Quadrature-axis magnetizing inductance
Lls	Armature leakage inductance
Rfd	Field resistance
Lfl	Field leakage inductance
Rkd	Direct-axis damper resistance
Lkdl	Direct-axis damper leakage inductance
Rkq	Quadrature-axis damper resistance
Lkql	Quadrature-axis damper leakage inductance
ω_r	Angular velocity of the rotor
J	Inertia coefficient
T_e	Electromagnetic torque
H	Inertia constant
F	Friction coefficient
V_{Lx}	Voltage across inductance x
V_{Cx}	Voltage across capacitance x
i_{Lx}	Current through inductance x
i_{Cx}	Current through capacitance x
P	Active power
Pg	Grid active power
Q	Reactive power
Qg	Grid reactive power
S	Apparent power
Sg	Grid apparent power
e g	Grid voltage vector
u	Converter output voltage vector
Ls	Series inductance of line filter
Rs	Series resistance of line filter
ω_g	Grid angular frequency
V_{dc}	DC link voltage
P_{dc}	DC link power
ρ	Air density

Results for DC transmission subsystem: This results is obtained with the following tuning of fuzzy controller.

CONCLUSION

In this paper a comparisons among different WECS have been provided with focus on direct driven systems. WECS direct drive system based on PMSG is highly recommended for regions with climate characterized be high wind speed and low/moderate temperatures while WECS direct drive system based on EESG is highly recommended for regions with climate characterized be high wind speed and high temperatures. Moreover, detailed modeling and analysis for WECS based on EESG has been provided including the control techniques for each subsystem. The simulation results showing the proper operation of speed controller for maximum power point extraction in the below rated wind speed and the pitch controller for power limitation in higher wind speeds. Furthermore, the response of the field voltage with the rotor speed variation reflecting the proper operation of the field excitation controller. For the grid side converter, vector control technique for synchronization to grid with controlled power has been implied. The simulation results showing that the control techniques are successfully regulate the Dc voltage and the reactive power and the grid connection requirements are fully adapted in all wind speed range.

REFERENCES

1. EWEA, 2012. Wind in Power: 2011 European Statistics, EWEA, Brussels.
2. EWEA, 2011b. The European Offshore Wind Industry Key Trends and Statistics 2010, EWEA, Brussels.
3. Polinder, H., F.A. van der Pijl, Gert-Jan de Vilderand Peter J. Tavner, 2006. Comparison of Direct-Drive and Geared Generator Concepts for Wind Turbines. IEEE Transactions on Energy Conversion, Vol: 21 (3).
4. Polinder, H., Sjoerd W.H. de Haan, Maxime R. Dubois and Johannes G. Slootweg, 2005. Basic Operation Principles and Electrical Conversion Systems of Wind Turbines. EPE J., 15 (4): 43-50.
5. Shaw, S. and S. Constantinides, 2012. Permanent Magnets: The Demand for Rare Earths. 8th International Rare Earths Conference November
6. Ion Boldea and S.A. Nasar, 1999. Electric Drives, CRC Press, Boca Raton.
7. Siegfried Heier, 1998. Grid Integration of Wind Energy Conversion Systems. John Wiley & Sons Ltd.
8. Slootweg, J.G., S.W.H. de Haan, H. Polinder and W.L. Kling, 2003. General Model for Representing Variable Speed Wind Turbines in Power System Dynamics Simulations. IEEE Transactions on Power Systems, Vol: 18 (1).
9. Krause, P.C., 1986. Analysis of Electric Machinery. McGraw-Hill,
10. Joos, G., L. Moran and P. Ziogas, 1991. Performance analysis of a PWM inverter VAr compensator. IEEE Trans. on Power Electronics, 6 (3): 380-391.
11. Ottersten, R. and J. Svensson, 1998. Vector current controlled grid connected PWM converter-deadbeat control and saturation strategies. 1998 IEEE Nordic Workshop on Power and Industrial Electronics, Espoo, Finland, Vol: 1.